PAPER

Comparative Analysis of Automatic Exudate Detection between Machine Learning and Traditional Approaches

Akara SOPHARAK[†a)], ***Nonmember***, **Bunyarit UYYANONVARA**[†], ***Member***, **Sarah BARMAN**[††], ***and*** **Thomas WILLIAMSON**[†††], ***Nonmembers***

SUMMARY To prevent blindness from diabetic retinopathy, periodic screening and early diagnosis are neccessary. Due to lack of expert ophthalmologists in rural area, automated early exudate (one of visible sign of diabetic retinopathy) detection could help to reduce the number of blindness in diabetic patients. Traditional automatic exudate detection methods are based on specific parameter configuration, while the machine learning approaches which seems more flexible may be computationally high cost. A comparative analysis of traditional and machine learning of exudates detection, namely, mathematical morphology, fuzzy c-means clustering, naive Bayesian classifier, Support Vector Machine and Nearest Neighbor classifier are presented. Detected exudates are validated with expert ophthalmologists' hand-drawn ground-truths. The sensitivity, specificity, precision, accuracy and time complexity of each method are also compared.

key words: *exudate, diabetic retinopathy, morphological, fuzzy c-means, naive Bayesian classifier, support vector machine, nearest neighbor classifier*

1. Introduction

For people with diabetes, diabetic retinopathy is the major cause of blindness. Early screening for diabetic retinopathy could improve the prognosis of proliferative retinopathy and reduce risk factor to lower the rate of blindness [1]–[4]. The appearance of microaneurysms, haemorrhages and exudates would represent the degree of disease. From visual inspection, exudates appear to be a yellowish or white colour with varying sizes, shape and locations. In this paper, we concentrate on exudate detection as a marker for the presence of macular edema. If the exudates extend into the macular area, vision loss can occur. In addition, the location of exudates based on macular position is important information for an ophthalmologist [5], [6]. They show the severity of disease, where exudates that appear closer to the macular indicate an increased severity of disease. A grid circle centred on the macular is added to provide improved diagnosis to the ophthalmologist [7]. Automatic exudate detection can assist ophthalmologists prevent and treat the disease more efficiently.

Many techniques have been employed to the exudate detection. B. Ege et al. [1] use thresholding to segment bright lesions and dark lesions, perform region growing, and then identify exudate regions with Bayesian, Mahalanobis and nearest neighbor classifiers. C. Sinthanayothin et al. [2] report the result of an automated detection of diabetic retinopathy using recursive region growing segmentation (RRGS). A. Osarah et al. [8], [9] use fuzzy c-means (FCM) clustering to segment colour retinal image, then neural network and support vector machines (SVMs) are used to separate exudate and non-exudate areas. T. Walter et al. [10] use morphological reconstruction techniques to detect contour of exudates. C.I. Sanchez et al. [11] combine colour and sharp edge features to detect exudates. D. Usher et al. [12] use a combination of RRGS and adaptive intensity thresholding to detect candidate exudate regions and a neural network is used to classify exudate and non-exudate. X. Zhang and O. Chutatape [13] use local contrast enhancement and FCM to segment candidate bright lesion areas. SVMs is also used to classify exudates and cotton wool spots.

Most techniques mentioned earlier work on images taken where the pupils of the patient are dilated in which the exudates and other retinal features are clearly visible. Good quality images are required. The examination time and effect on the patient could be reduced if the system can succeed on non-dilated pupils. Automatic exudate detection on images acquired without pupil dilation is investigated to provide decision support and reduce ophthalmologists' workload.

In previous work, we have proposed and evaluated method for automatic exudate detection using mathematical morphology techniques [7], [14], FCM [15], a combination of FCM and mathematical morphology [16], naive Bayesian classifier [17], SVMs classifier [18] and nearest neighbor classifier.

Because the nature of exudates appearing in the image varies in shapes and sizes, in order to detect exudates effectively using traditional approaches, such as mathematical morphology or fuzzy c-means (FCM) clustering, these methods require predefined setting of many parameters specific to the data set. Machine learning approaches may help eliminate the process of parameter configuration. However, it may be costly. In this paper, comparative analysis of both traditional and machine learning approaches, namely, mathematical morphology, FCM, naive Bayesian, SVMs and nearest neighbour classifier are presented. Section 2 briefly describes each detection method. Performances of

Manuscript received May 7, 2009.

[†]The authors are with Sirindhorn International Institute of Technology, Thammasat University, 131 Moo 5, Tiwanont Road, Bangkadi, Muang, Pathumthani, 12000, Thailand.

[††]The author is with Kingston University, Penrhyn Road, Kingston Upon Thames, Surrey, KT1 2EE, UK.

[†††]The author is with the Department of Ophthalmology, St Thomas' Hospital London, SE1 7EH, UK.

a) E-mail: akara@siit.tu.ac.th

DOI: 10.1587/transinf.E92.D.2264

classifiers are compared in Sect. 3. The paper is discussed and concluded in Sect. 4.

2. Method

All digital retinal images are taken without pupil dilation with a KOWA-7 non-mydriatic retinal camera with a 45□ field of view. The images are stored in JPEG image format files (.jpg) with lowest compression rates. The image size is 752×500 pixels at 24 bits per pixel.

In order to enhance the contrast of the image, a preprocessing method, as described in Sect. 2.1, is applied. Optic disc (OD) area has to be removed prior to the exudate detection and OD detection is described in Sect. 2.2. Classification experiments are clarified in Sect. 2.3.

2.1 Preprocessing

Each original RGB image is transformed to HSI colour space. A median filtering operation is then applied on intensity band to reduce noise. A contrast-limited adaptive histogram equalization (CLAHE) operator [19] is then applied to enhance the local contrast.

2.2 Optic Disc Detection

Exudate detection is our main purpose; however the optic disc has to be removed first because it has characteristics similar to exudates. It appears with similar intensity, colour and contrast to other features on the retinal images [20], [21]. Two separated techniques are used to ensure reliability of the optic disc detection. The first technique is based on a morphology method [7]. The optic disc is characterized by the largest high contrast among circular shape areas. Applying a grayscale closing operator on the intensity channel eliminates the vessels which may remain in the optic disc region. A flat disc-shaped structuring element with a fixed radius of eight is used. The resulting image is binarized and the image is then used as a mask. All the pixels in the mask are inverted before they are overlaid on the original image to remove candidate bright regions. The morphological reconstruction by dilation is then applied on the previous overlaid image. The difference between the original image and the reconstructed image is thresholded. The optic disc is then detected as the largest high contrast among circular shape area from the resulting image. On the second technique, the optic disc is detected by using entropy feature on preprocessed intensity image [15]–[17]. The local pixel intensity entropy measure is high when the region around a pixel is complex and low when it is smooth. After filtering with the entropy operator, Otsu's binarization algorithm [22] is applied to separate the complex regions from the smooth regions. The optic disc is then detected by the largest connected component whose shape is approximately circular. Intersect of result from both methods is used as an OD mask.

2.3 Exudate Detection

Exudate detection using mathematical morphology, FCM, a combination of FCM and mathematical morphology, naive Bayesian classifier, SVMs and nearest neighbor classifier are presented.

2.3.1 Mathematical Morphology

Similar to the optic disc detection steps using morphological method, high contrast vessels can be eliminated first by a closing operator before a local variation operator is applied. The resulting image is thresholded to get rid of all regions with low local variation. To ensure that all the neighboring pixels are also included in the candidate region, a dilation operator is also applied. The detected optic disc is then removed. The resulting image is used as a mask, showing all possible candidate regions of exudates. The exudate detection areas are obtained by applying a threshold operator to the difference between the original image and the reconstructed image.

2.3.2 Fuzzy C-Means Clustering

Four features are experimentally selected as input for FCM clustering. They are the intensity value after pre-processing, the standard deviation of intensity, hue and number of edge pixels from an edge image. For the number of edge pixels, we apply a Sobel edge operator then eliminate the strong edges arising from blood vessels and the optic disc using decorrelation stretch [23] on the red band. To determine the suitable number of cluster for FCM clustering, quantitative experiments with a parameter of a number of clusters varying from two to eight clusters are tested.

2.3.3 Combination of FCM and Mathematical Morphology Method

In this experiment we combine both FCM and Morphology for exudate detection. The image is coarsely segmented first using FCM clustering and then a fine segmentation using morphological reconstruction is applied. Four features from previous experiment are selected as input for clustering in FCM. The result from FCM clustering is a rough estimation of the exudates; a fine segmentation using morphological reconstruction is applied to get a better result.

2.3.4 Naive Bayesian Classifier

Fifteen features (including 4 features from previous experiments) are proposed to distinguish exudate pixel from non-exudate pixels. They are 1. the pixel's intensity value after preprocessing, 2. the standard deviation of the preprocessed intensity value, 3. the pixel's hue, 4. the number of edge pixel in a region around the pixel, 5. the average intensity of the pixel's cluster, 6. the size (measured in pixels) of

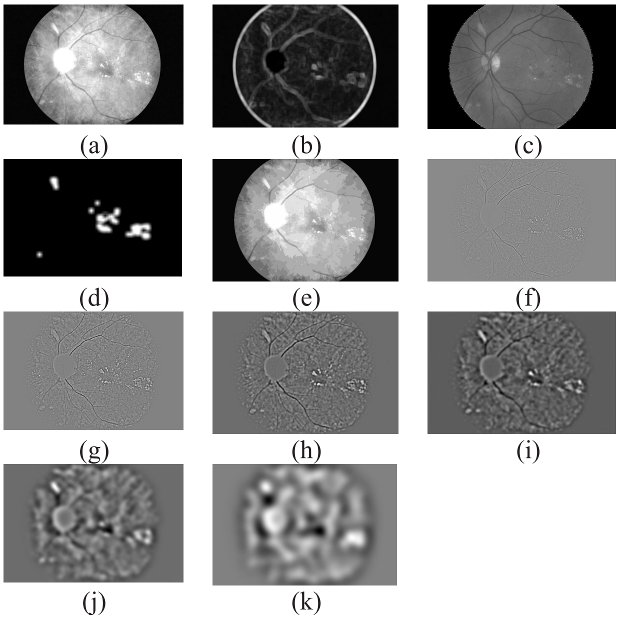

Fig. 1 Input features. (a) Preprocessed intensity. (b) Standard deviation of intensity. (c) Hue. (d) Number of edge pixels. (e) Cluster intensity. (f) DoG1. (g) DoG2. (h) DoG3. (i) DoG4. (j) DoG5. (k) DoG6.

the pixel's cluster, 7. the average intensity of the pixels in the neighborhood of the pixel's cluster, 8. the ratio between the size of the pixel's cluster and the size of the optic disc, 9. the distance between the pixel's cluster and the optic disc and six Difference of Gaussian (DoG) filter responses with six different standard deviation values, namely DoG1, DoG2 and so on. Examples of some of the features are shown in Fig. 1. Before feature selection or classification, we z-scale (transform to a mean of 0 and a standard deviation of 1) all 15 features using the statistics of each feature over the training set.

Feature selection proceeds as follows. We first estimate the model from a training set using all features then evaluate the resulting classifier's performance on a separate test set. Then we iteratively delete features until the average of the precision and recall (PR, see next section) stops improving. On each step, for each feature, we delete that feature from the model, train a new classifier, and evaluate its performance on the test set. The PR of the best such classifier is compared to the PR of the classifier without deleted features. If PR improves, we permanently delete that feature then repeat the process. Finally, the best feature set and classifier are retained.

2.3.5 Support Vector Machines Classifier

SVMs map training data into a high-dimensional feature space in which we can construct a separating hyper-plane maximizing the margin, or distance from the hyperplane to the nearest training data points. The ν-SVM [24] with a radial basis function (RBF) kernel is used in which the parameter $\nu \in [0, 1]$ controls how many support vectors are allowed to lie on the wrong side of the separating hyper-plane.

We use the best feature set obtained from naive Bayesian classifier as an initial feature set for the SVM. We then add features to the SVM classifier one at a time and compare the PR of each classifier to that of the previous classifier. The first feature added in is always the last feature removed as the same sequence of previous naive Bayesian classifier's feature selection process. The feature-adding process is repeated until all features are added back. The best feature set is the set which provides the highest PR.

2.3.6 Nearest Neighbor Classifier

The nearest neighbor classifier simply classifies a test instance with the class of the nearest training instance according to two distance measures, Mahalanobis and Euclidean distance.

2.3.7 Macular Detection

The macular is detected from the intensity image by the darkest region on the retinal image; it is not always the case due to high illumination. The typical characteristics of the macular (for example, it is within the neighborhood of the optic disc) is also used to detect the macular more accurately. The darkest area in the neighborhood of the optic disc (approximately 2.5 times the diameter of the optic disc from the centre of optic disc) is considered as a macular. A Macular grid is drawn according to the ETDRS report [5] with a radius of one third of the optic disc diameter, one optic disc diameter and two optic disc diameters respectively.

2.3.8 Performance Measurement

We evaluate performance on the test set quantitatively by comparing the classifier's result to ground truth. To obtain ground truth for each image, we used image processing software to hand label candidate exudate regions, then two ophthalmologists are asked to verify or reject each candidate region.

To evaluate classifier performance, we use sensitivity, specificity, precision, PR and accuracy on a per-pixel basis. All measures can be calculated based on four values, namely the true positive (TP) rate (the number of exudate pixels correctly detected), the false positive (FP) rate (the number of non-exudate pixels wrongly detected as exudate pixels), the false negative (FN) rate (the number of exudate pixels not detected), and the true negative (TN) rate (the number of non-exudate pixels correctly identified as non-exudate pixels).

Sensitivity (recall) is the percentage of the actual exudate pixels that are detected, and specificity is the percentage of non-exudate pixels that are correctly classified as non-exudate pixels. Precision is the percentage of detected pixels that are actually exudate, and PR is the average of the precision and recall. Accuracy is the overall per-pixel success rate of the classifier.

3. Results

In this section, the experiment result of exudate detection using mathematical morphology techniques, FCM, a combination of FCM and mathematical morphology, naive Bayesian, SVMs and nearest neighbor classifier is presented. A population of 60 retinal images comprised of 40 images with exudates and 20 images without exudates are tested on an AMD Athlon 1.25 GHz PC using MATLAB for mathematical morphology, FCM and FCM with morphology. For naive Bayesian and SVM, we use 29 images for training and 30 images comprised of 10 images with exudates and 20 images without exudates for testing. All exudate pixels and equal number of non-exudate pixels (randomly selected) are included in the training set. Over all 29 training images, we obtained 115,867 examples of positive (exudate) pixels and an equal number of negative (non-exudate) pixels. Our 10 test images together contain 42,909 exudate pixels. A naive Bayesian is tested on Weka data mining software running on a standard PC while SVMs and nearest neighbor are tested on a 20-node Gnu/Linux Xeon cluster. Because all the algorithms run on different platforms, performance of each algorithm cannot be measured and compared using running time. Computation complexity of each algorithm is compared instead as in Table 1. Finally, detected exudates are compared with the ophthalmologist' hand-drawn ground-truth images for verification.

Table 1 Time complexity (for one image).

Classifier	Training Time complexity	Testing Time complexity
Mathematical morphology	-	$O(n^2 i)$
Fuzzy c-means (8 clusters)	-	$O(nfc^2 i)$
Fuzzy c-means (8 clusters) + Morphology	-	$O(nfc^2 i)$ + $O(n^2 i)$
Naive Bayesian	$O(mf)$	$O(nf)$
Support vector machines	$O(m^2 f^2)$	$O(nfs)$
Nearest neighbor	$O(1)$	$O(nft)$

* m is number of training data (number of training pixels), n is number of testing data (number of testing pixels), i is number of iteration, c is number of cluster, f is number of features, s is number of support vectors and t is number of training points.

3.1 Experiment 1: Mathematical Morphology

Each image takes approximately 3 minutes to process, including the optic disc removal step which takes around 1 minute. For our data set, the sensitivity, specificity, precision, PR and accuracy are 80%, 99.46%, 51.78%, 65.89% and 99.29%, respectively.

3.2 Experiment 2: Fuzzy C-Means Clustering

The approximate time taken for running the whole process for each image with number of cluster = 2, 3, 4, 5, 6, 7 and 8 are 1.5, 2, 5, 7, 10.5, 15, and 18 min, respectively. With number of cluster equal 8, the sensitivity, specificity, precision, PR and accuracy are 97.29%, 85.43%, 51.62%, 5.94% and 85.62%, respectively.

3.3 Experiment 3: Fuzzy C-Means Clustering and Mathematical Morphology Method

Each image takes approximately 18 minutes for FCM clustering and another 3 minutes for morphological reconstruction. After fine segmentation, most of the classified exudate regions are true exudate pixels, which give a smaller true positive value; however, it also reduces the false positive value because misclassification of non-exudate pixels is also lower. Figure 2 displays the comparison of exudate detection from the experiment 3.2, result of FCM clustering followed by morphological reconstruction and a ground-truth image. It is found that this method detects exudates successfully with sensitivity, specificity, precision, PR and accuracy of 87.28%, 99.24%, 42.77%, 65.02% and 99.11%, respectively.

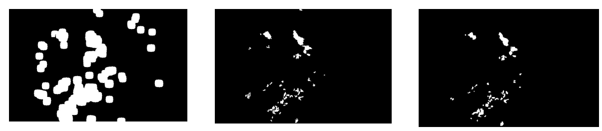

(a) (b) (c)

Fig. 2 Comparison of exudates detection. (a) Result from FCM clustering. (b) Fine segmentation using morphological reconstruction (c) Ground truth image.

3.4 Experiment 4: Naive Bayesian Classification

We used Weka data mining software [25] running on a standard PC for feature discretization and naive Bayesian classification. We fit the naive Bayesian model to the training set using all 15 features. The resulting classifier had an overall per-pixel sensitivity, specificity, precision, PR and accuracy of 95.84%, 96.56%, 33.49%, 64.67% and 96.55%, respectively.

When we removed features from the classifier one by one and compared the resulting PR to PR obtained on the previous feature set, we obtained the best PR value by deleting cluster intensity, presumably due to its redundancy with the pixel intensity feature. We continued this process until the PR stopped improving. Finally, the best classifier contained six features: 1. the pixel's intensity after preprocessing, 2. the standard deviation of the preprocessed intensities in a window around the pixel, 3. the pixel hue, 4. the number of edge pixels in a window around the pixel, 5. the ratio between the size of the pixel's intensity cluster and the optic disc, and 6. DoG4.

3.5 Experiment 5: Support Vector Machine Classification

We used libSVM's [26] implementation of the ν-SVM with the radial basis function kernel on a 20-node Gnu/Linux Xeon cluster for training and testing SVM classifiers. For a given feature set, to find optimal hyperparameters (ν, the tolerance for misclassified training examples, and γ, the width of the radial basis function) for the SVM, we performed a grid search, retaining the parameter values for which test set accuracy is maximized. We then added features back into the classifier one by one and repeated the grid search for each feature set combination. We found that PR fluctuated as we performed feature inclusion, so we continued including features until all 15 features are included. The best performance is obtained using 10 features: 1. pixel's intensity after preprocessing, 2. standard deviation of the preprocessed intensities in a window around the pixel, 3. pixel hue, 4. number of edge pixels in a window around the pixel, 5. ratio between the size of the pixel's intensity cluster and the optic disc, 6. distance between the pixel's cluster and the optic disc, 7. DoG1, 8. DoG2, 9. DoG4, and 10. DoG6, with $\nu = 0.002$ and $\gamma = 0.98$. This classifier has a sensitivity of 92.28%, specificity of 98.52%, precision of 53.05%, and PR of 72.67%. The overall accuracy is 98.41%.

3.6 Experiment 6: Nearest Neighbor Classification

Nearest neighbor classifier with Euclidean and Mahalanobis distance metrics are used as our baseline for comparison. To be able to compare with naive Bayesian and SVM classifiers, we used the best feature sets obtained for naive Bayesian and the SVM. On the best feature set obtained from the naive Bayesian classifier, the nearest neighbor classifiers have a PR of 61.54% and 61.81%, respectively. On the best feature set obtained from the SVM classifier, the nearest neighbor classifier achieved a PR of 65.15% and 64.99%, respectively. The results indicate that the naive Bayesian and SVM classifiers perform substantially better in PR than the nearest neighbor classifier. In addition, the nearest neighbor classifier using the best feature set obtained from the SVM classifier performs better than that using the best feature set for the naive Bayesian classifier.

3.7 Experiment 7: Macular Detection

The system also detects the macular region in order to provide the ophthalmologists with the distance information between the detected exudates and the macular. The exudates within the inner circle will affect the vision of patients more than the ones outside it. As shown in Fig. 3 (a), exudates are present nearer to the macular than exudates in Fig. 3 (b). This indicates that the exudates in Fig. 3 (a) will be more harmful to vision than those in Fig. 3 (b).

3.8 Comparing Classifier Results

An example image of a diabetic retinopathy retinal image and the detected result superimposed on the original image are shown in Fig. 4. Graphical representations of PR and precision values are shown in Fig. 5. Resulting images of exudate detection from all experiments are shown in comparison in Fig. 6 (as examples of good detection) and Fig. 7 (as examples of false detection). The training performances and testing performance are compared in Table 2 and Table 3, respectively. Classifier selection factor is also presented in Table 4.

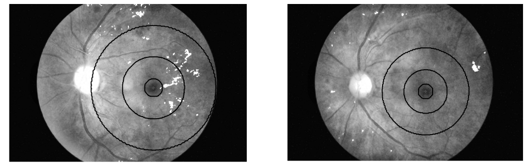

(a) (b)

Fig. 3 (a) and (b) Macular grid centred on the macular, superimposed on the exudate detection result.

(a) (b) (c)

Fig. 4 Exudates detection. (a) Original images. (b) Detected result. (c) Result of (b) superimposed on image (a).

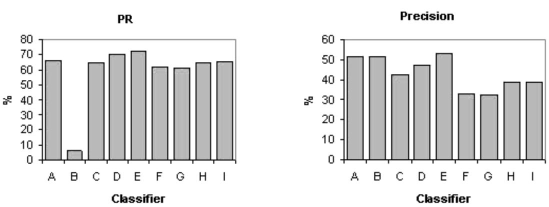

(a) (b)

Fig. 5 Graphical representation of PR and precision values of *A* (mathematical morphology), *B* (FCM), *C* (FCM with morphology), *D* (naive Bayesian), *E* (SVMs), *F* (nearest neighbor with Euclidean distance on best feature set obtained from naive Bayesian, *G* (nearest neighbor with Mahalanobis distance on best feature obtained from naive Bayesian, *H* (nearest neighbor with Euclidean distance on best feature set obtained from SVMs, *I* (nearest neighbor with Mahalanobis distance on best feature set obtained from SVMs.

4. Conclusion and Discussion

In this paper we describe the comparative results of automatic exudate detection using traditional and machine learning approaches. Mathematical morphology, FCM, combination of FCM and morphology method, naive Bayesian classifier, SVMs classifier and nearest neighbor classifier are investigated.

The weakness of traditional exudate detection is that they require many predetermined features while the machine learning approaches takes time to learn and search for the best feature set. Pre-defined number of cluster is also the weakness of FCM clustering. The suitable number of clusters is dependent on the requirements of the ophthalmologist

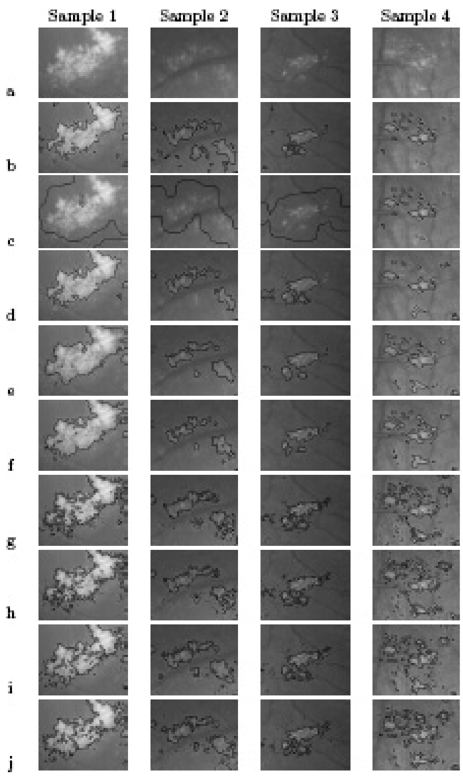

Fig. 6 Result of exudate detection. (a) Original images (b) Morphology classification results. (c) FCM classification results. (d) FCM with Morphology classification results. (e) Naive Bayesian classification results. (f) SVM classification results. (g) Nearest Neighbor (Euclidean distance) classification results on best feature set obtained from Naive Bayesian. (h) Nearest Neighbor (Mahalanobis distance) classification results on best feature obtained from Naive Bayesian. (i) Nearest Neighbor (Euclidean distance) classification results on best feature set obtained from SVM. (j) Nearest Neighbor (Mahalanobis distance) classification results on best feature set obtained from SVMs.

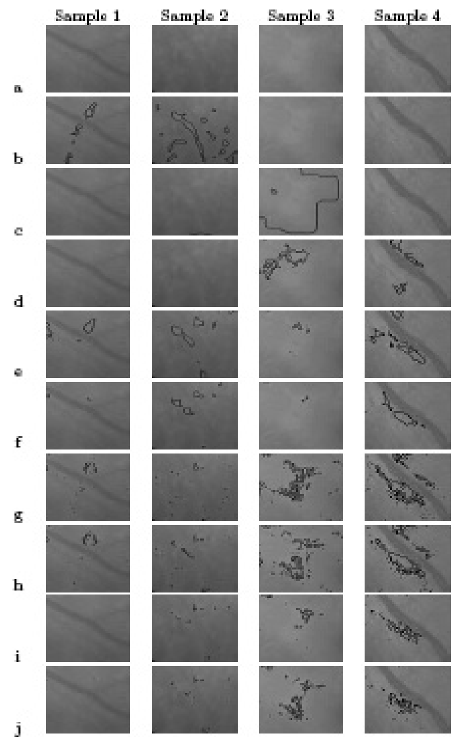

Fig. 7 Example false detection of exudates on choroidal blood vessel (sample 5 and 6) and on nerve fiber (sample 7 and 8). (a) Original images. (b) Morphology classification results. (c) FCM classification results. (d) FCM with Morphology classification results. (e) Naive Bayesian classification results. (f) SVMs classification results. (g) Nearest Neighbor (Euclidean distance) classification results on best feature set obtained from Naive Bayesian. (h) Nearest Neighbor (Mahalanobis distance) classification results on best feature obtained from Naive Bayesian. (i) Nearest Neighbor (Euclidean distance) classification results on best feature set obtained from SVM. (j) Nearest Neighbor (Mahalanobis distance) classification results on best feature set obtained from SVMs.

and the application. If the application requires high PPV or PLR, such as an application of an automatic quantitative measurement of exudates, $n = 8$ may be chosen because it gives a higher accuracy with low false positive value. However, if the applications do not require such a high accuracy, such as an application of ophthalmologists' visual aid in exudate detection where the computer enhances the image quality and shows an approximate location of the exudates and the decision is still made by an expert ophthalmologist, $n = 2$ is recommended. Also, with this parameter, $n = 2$, the system runs faster. The naive Bayesian and SVM classification required learning phase which takes time. Many parameters are also used in SVM classification and they can affect the classification accuracy. Computational costs for SVMs are very expensive.

Among all classifiers, our experimental results show that the mathematical morphology method achieves highest specificity and accuracy with 99.46% and 99.29%, respectively. In the other hand, the mathematical morphology method achieves lowest sensitivity with 80%. As shown in the result images of exudate detection using FCM, most of exudates are detected. FCM achieves highest sensitivity of 97.29%, and lowest specificity and accuracy of 85.43% and 85.62% at the same time. Rough exudates detection using only FCM achieves very low PR value because of high false positive values. The PR value is improved when fine exudates detection using mathematical morphology technique is combined to FCM. Among all classifiers we use in this paper, SVMs classifier achieves the highest PR with 72.67%.

Considering time complexity, for SVMs the training time is related to the number of support vectors, which depend on the dataset and on the nonlinear mapping from input space to the feature space but SVM's time complexity of testing process equal nearest neighbor's if number of supports is equal to number of training points. We find that the SVM classifier tends to delineate exudate boundaries more accurately with fewer false detection. Retinal structures that share some characteristics with exudates can be incorrectly detected as exudates. High contrast choroidal blood vessels appearing in the retinal background and nerve fiber can be incorrectly detected as exudates. And due to the light reflection, there are some high intensity artifacts near large retinal blood vessels. These artifacts are one of the main causes of false classification of some normal images.

Table 2 Training performance.

Classifier	Sensitivity (%)	Specificity (%)	Precision (%)	PR (%)	Accuracy (%)
Naive Bayesian	94.53	89.19	89.74	92.13	91.86
Support vector machines	92.06	94.92	94.77	93.41	93.49

Table 3 Performance comparison.

Classifier	Sensitivity (%)	Specificity (%)	Precision (%)	PR (%)	Accuracy (%)
Mathematical morphology	80.00	99.46	51.78	65.89	99.29
Fuzzy c-means (8 clusters)	97.29	85.43	51.62	5.94	85.62
Fuzzy c-means (8 clusters) + Morphology	87.28	99.24	42.77	65.02	99.11
Naive Bayesian	93.38	98.14	47.51	70.45	98.05
Support vector machines	92.28	98.52	53.05	72.67	98.41
Nearest neighbor on best feature set for naive Bayesian (Euclidean)	90.48	96.62	32.60	61.54	96.51
Nearest neighbor on best feature set for naive Bayesian (Mahalanobis)	90.44	96.71	33.18	61.81	96.60
Nearest neighbor on best feature set for SVM (Euclidean)	91.44	97.40	38.86	65.15	97.29
Nearest neighbor on best feature set for SVM (Mahalanobis)	91.11	97.41	38.87	64.99	97.30

Table 4 Classifier selection factor.

Classifier	Parameters sensitive	Require Learning phase	High Computation cost	Require high computer system
Mathematical morphology	Yes			
Fuzzy c-means (8 clusters)	Yes			
Fuzzy c-means (8 clusters) + Morphology	Yes			
Naive Bayesian		Yes		Yes
Support vector machines	Yes	Yes	Yes	Yes
Nearest neighbor				Yes

Mathematical morphology is a simple method and computationally low cost but it does not achieve good sensitivity. FCM clustering can detect most of the exudate regions, however, lots of false positive are also high at the same time. Additionally, sensitivity and specificity are depending on the number of clusters which has to be predefined. Using FCM clustering followed by mathematical morphology reconstruction, gives higher accuracy with a lower false positive value. Even though, Naive Bayesian and SVM which are supervised classifiers do not require predefined features, they are computationally expensive during training process. The SVMs classifier is also sensitive to parameter modification but it gains higher precision value.

Performances of all exudate classifiers discussed in this paper depend on optic disc and vessel detection. In future work, we plan to explore using the system as a practical aid to help ophthalmologists for diabetic retinopathy screening.

Acknowledgments

We thank Thammasat University Hospital for the images and ground truth data used in these experiments. This research is funded by the Thailand National Electronics and Computer Technology Center (NECTEC).

References

[1] B. Ege, O. Hejlesen, O. Larsen, K. Moller, B. Jennings, D. Kerr, and D. Cavan, “Screening for diabetic retinopathy using computer based image analysis and statistical classification,” Comput. Meth. Programs Biomed., vol.62, pp.165–175, 2000.

[2] C. Sinthanayothin, J.F. Boyce, T.H. Williamson, H.L. Cook, E. Mensah, S. Lal, and D. Usher, “Automated detection of diabetic retinopathy on digital fundus image,” J. Diabet. Med., vol.19, pp.105–112, 2002.

[3] G.G. Gardner, D. Keating, T.H. Williamson, and A.T. Elliott, “Automatic detection of diabetic retinopathy using an artificial neural network: A screening tool,” British Journal of Ophthalmology, vol.80, pp.940–944, 1996.

[4] Z. Liu, O. Chutatape, and S.M. Krishna, “Automatic image analysis of fundus photograph,” IEEE Conf. on Engineering in Medicine and Biology, vol.2, pp.524–525, 1997.

[5] E.T.D.R.S.R. Group, “Grading diabetic retinopathy from stereoscopic color fundus photographs: An extension of the modified airlie house classification, etdrs report number 10,” Ophthalmology, vol.98, pp.786–806, 1991.

[6] M.D. Davis, S.B. Bressler, L.P. Aiello, N.M. Bressler, D.J. Browning, C.J. Flaxel, D.S. Fong, W.J. Foster, A.R. Glassman, M.E.R. Hartnett, C. Kollman, H.K. Li, H. Qin, and I.U. Scott, “Comparison of time-domain oct and fundus photographic assessments of retinal thickening in eyes with diabetic macular edema,” Invest. Ophthalmol. Vis. Sci., vol.49, pp.1745–1752, 2008.

[7] A. Sopharak, B. Uyyanonvara, S. Barman, and T.H. Williamson, "Automatic detection of diabetic retinopathy exudates from non-dilated retinal image using mathematical morphology methods," Computerized Medical Imaging and Graphics, vol.32, pp.720–727, 2008.

[8] A. Osareh, M. Mirmehdi, B. Thomas, and R. Markham, "Automatic recognition of exudative maculopathy using fuzzy c-means clustering and neural networks," in Medical Image Understanding and Analysis Conference, ed. E. Claridge and J. Bamber, pp.49–52, BMVC Press, UK, 2001.

[9] A. Osareh, M. Mirmehdi, B.T. Thomas, and R. Markham, "Comparative exudate classification using support vector machines and neural networks," MICCAI '02: Proc. 5th International Conference on Medical Image Computing and Computer-Assisted Intervention-Part II, pp.413–420, Springer-Verlag, London, UK, 2002.

[10] T. Walter, J.C. Klevin, P. Massin, and A. Erginay, "A contribution of image processing to the diagnosis of diabetic retinopathy - detection of exudates in color fundus images of the human retina," IEEE Trans. Med. Imaging, vol.21, no.10, pp.1236–1243, 2002.

[11] C.I. Sanchez, R. Hornero, M.I. Lopez, and J. Poza, "Retinal image analysis to detect and quantify lesions associated with diabetic retinopathy," IEEE Conf. on Engineering in Medicine and Biology Society, vol.1, pp.1624–1627, 2004.

[12] D. Usher, M. Dumskyj, M. Himaga, T.H. Williamson, S. Nussey, and J. Boyce, "Automated detection of diabetic retinopathy in digital retinal images: A tool for diabetic retinopathy screening," J. Diabet. Med., vol.21, pp.84–90, 2004.

[13] Z. Xiaohui and O. Chutatape, "Detection and classification of bright lesions in colour fundus images," IEEE Conf. on Image Processing, vol.1, pp.139–142, 2004.

[14] A. Sopharak and B. Uyyanonvara, "Automatic exudates detection on thai diabetic retinopathy patients' retinal images," Proc. 2006 ECTI International Conference, pp.709–712, 2006.

[15] A. Sopharak and B. Uyyanonvara, "Automatic exudates detection from non-dilated diabetic retinopathy retinal image using fuzzy c-means clustering," Proc. Third WACBE World Congress on Bioengineering, 2007.

[16] A. Sopharak and B. Uyyanonvara, "Automatic exudates detection from diabetic retinopathy retinal image using fuzzy c-means and morphological methods," Conf. on Advances in Computer Science and Technology, pp.359–364, 2007.

[17] A. Sopharak, K.T. New, Y.A. Moe, M.N. Dailey, and B. Uyyanonvara, "Automatic exudates detection with a naive bayes classifier," Imaging in the Eye IV, 2008.

[18] A. Sopharak, K.T. New, Y.A. Moe, M.N. Dailey, B. Uyyanonvara, and S. Barman, "Automatic exudates detection with a support vector machine classifier," Proc. 2008 International Conference on Embedded Systems and Intelligent Technology, pp.139–142, 2008.

[19] R.C. Gonzalez, R.E. Woods, and S.L. Eddins, Digital Image Processing Using Matlab, Prentice Hall, Upper Saddle River, NJ, USA, 2003.

[20] A. Osareh, M. Mirmehdi, B. Thomas, and R. Markham, "Automated identification of diabetic retinal exudates in digital colour images," Br. J. of Ophthalmology, vol.87, pp.1220–1223, 2003.

[21] C. Sinthanayothin, J.F. Boyce, H.L. Cook, and T.H. Williamson, "Automated localization of the optic disc, fovea, and retinal blood vessels from digital colour fundus images," Br. J. Ophthalmal, vol.83, pp.231–238, 1999.

[22] N. Otsu, "A threshold selection method from gray-level histogram," IEEE Trans. Syst. Man Cybern., vol.9, no.1, pp.62–66, 1979.

[23] S.L. Phung, A. Bouzerdoum, and D. Chai, "Skin segmentation using color pixel classification: Analysis and comparison," IEEE Trans. Pattern Anal. Mach. Intell., vol.27, no.1, pp.148–154, 2005.

[24] B. Scholkopf, A.J. Smola, R.C. Williamson, and P.L. Bartlett, "New support vector algorithms," Neural. Comput., vol.12, no.5, pp.1207–1245, 2000.

[25] I.H. Witten and E. Frank, Data Mining: Practical machine learning tools and techniques, Morgan Kaufmann, San Francisco, 2005.

[26] C.C. Chang and C.J. Lin, "Libsvm: A library for support vector machines," 2001. Software available at http://www.csie.ntu.edu.tw/cjlin/libsvm

Akara Sopharak received her BSc and MSc degrees in computer science from Burapha University and Mahidol University, Thailand, in 1998 and 2002 respectively. She is currently a doctor degree student at Sirindhorn International Institute of Technology, Thammasat University, Thailand. She is also an instructor with Faculty of Science and Arts of Burapha University. Her research interests are medical image processing and image analysis.

Bunyarit Uyyanonvara received his PhD in Medical Image Analysis from King's College, London in 2000 and a BSc of Science (1st Class Honours) from Prince of Songkhla University, Thailand. He is now an assistant professor at Sirindhorn International Institute of Technology, Thammasat University, Thailand.

Sarah Barman received her PhD in Optical Physics from King's College, London in 1996. She obtained an MSc in Applied Optics from Imperial College London and a BSc in Physics from Essex University. She is now a Principle Lecturer at the Digital Imaging Research Centre in the Faculty of Computing, Information Systems and Mathematics at Kingston University.

Thomas Williamson is a consultant ophthalmologist St Thomas' hospital, London, UK, with a specialist interest in vitreoretinal surgery. He trained in Aberdeen, Glasgow, Cambridge and London. Author of a major text book on vitreoretinal surgery over 100 publications in international research journals. 5000 vitreoretinal operations performed in 10 years.